Progress in Organic Coatings 191 (2024) 108424

Contents lists available at ScienceDirect

Progress in Organic Coatings

journal homepage: www.elsevier.com/locate/porgcoat

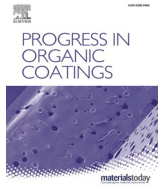

Self–healing core–shell nanofibers for corrosion protective coatings for offshore structures

Natalia C.M. Spera [a,*], Cristina Salazar-Castro [b], Paula C. Álvarez de Eulate [b], Yury V. Kolen'ko [a], Juliana P.S. Sousa [a]

[a] Nanochemistry Research Group, International Iberian Nanotechnology Laboratory, Braga 4715–330, Portugal
[b] Centro Tecnológico Lurederra, Los Arcos 31210, Navarra, Spain

ARTICLE INFO

Keywords:
Self–healing coatings
Core–shell nanofibers
Anticorrosive coatings
Advanced protective coatings
Wind renewable energy

ABSTRACT

Protective coatings are used as a corrosion mitigation strategy in many industries. However, damages on transport, installation, and during the service life can expose the metal, leading to failures. Self–healing materials can address this issue by recovering their properties and functionality post-damage. Herein, it was developed an extrinsic self-healing coating by incorporating core–shell nanofibers obtained by coaxial electrospinning. Overcoming the non–spinnability of organosilane compounds, a one–trigger component healing agent was achieved. Additionally, scalability limitations for self-healing coatings were defeated by implementing a viable technique for large-scale structures – Spray painting. The final protective and healing behaviour was investigated by electrochemical and salt spray tests. Following damage, the immediate healing response reached 97.5 %, initiated solely by water. Low capacitance values for the developed coating indicated a robust protective barrier. Furthermore, the self-healing coating efficiently protected steel from corrosion in the salt spray test. The results obtained showed a promising future in using core–shell nanofibers to enhance the durability and protective capabilities of coatings for offshore facilities.

1. Introduction

An electrochemical corrosion process is a challenging problem for many industries that heavily rely on the usage of metallic materials in corrosive environments, especially, for wind offshore facilities, which yearly cost billions on maintenance and repairs of metallic structures [1]. The most common strategy against corrosion is the employment of advanced organic–based corrosion resistant coatings to protect offshore metallic structures [2,3]. Unfortunately, the transportation and installation of offshore wind turbines is a complex process conducted over several steps. During the entire process, corrosion-resistant coating of metallic structures sometimes suffers undesirable mechanical damages, and hence, when the structure is placed in the maritime environment, the corrosion process initiates *via* penetration of corrosive media at the damaged point [4]. Notably, the wind offshore turbines generally last for 20 years and could be extendable to 25 years depending on maintenance protocols [5], wherein the maintenance costs increase as the structure ages [6]. To extend the lifetime of metallic offshore structures while simultaneously decreasing their maintenance costs, there is a growing interest within the research community and industry in the employment of robust self–healing coatings, affording an immediate and efficient self–recovery of the damaged area [7].

Self–healing mechanisms can be classified into intrinsic and extrinsic [8,9]. Intrinsic mechanism refers to the coating polymers themselves, exclusively healing after the application of external factors, such as UV radiation or temperature [7,10,11]. In contrast, the extrinsic mechanism has an autonomous self–healing response to the damage [12–14]. More specifically, the healing agent is typically encapsulated in the carrier and dispersed through the coating matrix. The healing of the damaged area occurs once the shell of the container is breached by a mechanical trigger (*i.e.*, damage), and then the reparative functional materials are released from the core and heal the damaged area of the coating [15,16]. Nevertheless, the depletion of the healing agent in the capsules leads to only a singular healing event, and the low uniformity of the capsule dispersion within the coating is also a concern [10,17]. Besides capsules, another extrinsic and highly interesting self–healing system is core–shell fibres. The fibres, randomly oriented through the coating matrix form a vascular–like system; thus, guaranteeing that the self–healing will occur

* Corresponding author.
E-mail address: natalia.spera@inl.int (N.C.M. Spera).

https://doi.org/10.1016/j.porgcoat.2024.108424
Received 6 December 2023; Received in revised form 25 March 2024; Accepted 26 March 2024
Available online 12 April 2024

at any damaged zone of the protective coating [18]. Moreover, as a result of the interconnected vascular–like structure, the healing agent in the core–shell fibres can also flow to the depleted areas, thus allowing multiple healing events [19–21], in contrast to singular healing events usually offered by capsules. Besides that, tubular containers incorporated into the coatings system do not compromise the integrity of the coating, which are both suitable for thin and thick coatings [22].

The most promising technique to obtain fibres with self–healing properties is the coaxial electrospinning of core–shell polymeric systems. However, the dispersion of the as–synthesized fibres in the coating remains an outstanding formulation challenge. For this reason, most of the fibre–based vascular–systems reported in the literature for the corrosion protective coatings are prepared by the direct impregnation method, embedding the polymeric matrix into fibres [19,20], pressed composites [23], or spin coating [24]. In addition, in the literature, it is usually reported the situation when two complementary electrospun fibres are simultaneously employed, namely, the one, which is filled with a monomer, and the complementary one, which is filled with the respective polymerization catalyst [19,20,25]. Mechanical damage will disrupt the shell of both fibres, and the two released compounds will then react to heal the damaged site. The requirement of producing two different fibrous materials is somewhat disadvantageous from the preparation and coating formulation points of view, in addition to the probability of not having both monomer and catalyst compounds at the same damaged site at the required concentrations. Accordingly, many researchers seek solutions for single-component self–healing material that does not require a reaction with the catalyst in the coating matrix. For example, there are few studies based on single-component coatings containing organic compounds with a pH change trigger instead of the polymerization catalyst [26–30].

Recently, water reactive organosilanes have gained great attention as single-component self–healing materials [31–33], which heals after exposure to ambient moisture and form a solid–like film using crosslink polymerization. In particular, silyl esters have been proven to have an excellent healing capability in the presence of water [34]. After the mechanical damage of the container, silyl ester material undergoes moisture–assisted hydrolysis, forming a hydrophobic layer on the metallic surface that protects the metal against the corrosive environment [35]. Such self–healing system could be highly beneficial for wind offshore applications, possessing a constant moisture environment needed for the hydrolysis of silyl ester. However, the preparation and investigation of silyl–ester–containing self–healable core–shell fibres by electrospinning is limited in the literature.

The purpose of this study was to apply this organosilane compound inside a fibrous morphology, and to investigate its self-healing attributes when incorporated into a coating matrix. Additionally, our aim was also to address the constraints hindering the limitations of the use of the self-healing technology regarding the up-scaling processes by implementing a viable coating technique that has already demonstrated efficacy in large-scale structures. In this context, we synthesize, through coaxial electrospinning, core–shell fibres of an organosilane based on silyl ester. The formulated novel self–healing protective coating afforded spray–painting capability, which is highly challenging for fibre–based systems [36]. Lastly, the self–healing ability and corrosion-protective properties of the newly developed coating were investigated by electrochemical analysis and salt spray test after an artificial damage.

2. Material and methods

2.1. Synthesis of silyl ester healing agent

The synthesis of the water–reactive organosilane healing agent was carried out using the procedure reported by García et al. [35]. Briefly, oleic acid (OA, 90 %, Sigma Aldrich), triethylamine (TEA, 99 %, Sigma Aldrich) and extra dry toluene (99.8 %, Enzymatic) were mixed in a ratio of 1:0.48:5.23 (*v*/v/v) under an inert nitrogen atmosphere using magnetic stirring, and then, the resultant mixture was immersed into an ice bath. Following, a solution of chloro(dimethyl)octylsilane (97 %, Sigma Aldrich) in extra dry toluene with a 1:0.75 (*v*/v) ratio was added dropwise to the previous mixture over a 1 h period. Subsequently, the ice bath was removed, and the mixture was stirred overnight at room temperature. The resulting octyl(dimethyl)silyloleate product was filtered, washed twice with toluene, and dried for 2 h in a rotary evaporator, thus affording a silyl ester compound in powder form.

2.2. Preparation of core-shell fibres

The core polymeric solution was prepared by mechanical dispersion for 1 h under ambient conditions of 15 % synthesized silyl ester powder in a mixed solution containing polyvinylpyrrolidone (PVP, $M_n = 40{,}000$, Sigma Aldrich) and extra dry N, N–dimethylformamide (DMF, 99.8 %, Sigma Aldrich) with 1:1.5 (v/v) ratio. The viscosity of the resultant core polymeric solution was around 700–800 cP, as measured by HAAKE Viscotester E (Thermo Scientific), while the electrical conductivity was measured to be *ca.* 80 μS/cm using a SevenMulti S40—K benchtop meter (Mettler Toledo). The shell polymeric solution was composed of 8 % polyacrylonitrile (PAN, $M_w = 150{,}000$, Sigma−Aldrich) in DMF. The viscosity of the solution was around 400–500 cP while the conductivity was measured to be 20 μS/cm. Finally, the core–shell fibres were synthesized by coaxial electrospinning of the aforementioned core and shell polymeric solutions using a Fluidnatek LE–50 electrospinning instrument (Bioinicia) with a vertical collector at 25 cm, a voltage of 21–23 kV and flow rates of 1.6 and 0.8 ml/h for the shell and the core solutions, respectively.

2.3. Characterization

The morphology of the materials was investigated by Transmission Electron Microscopy (TEM) using a JEM–2100 microscope (JEOL) and by Scanning Electron Microscopy (SEM) using a Quanta 650 FEG microscope (FEI). Fibres diameter measurements were then obtained from SEM micrographs using image-processing software ImageJ (NIH). The chemical properties of the materials were determined by Fourier−transform Infrared Spectroscopy (FTIR) using a Vertex 80v spectrometer (Bruker). The thermal stability of the materials was analysed by Thermogravimetric analysis (TGA) using the TGA/DSC 1 STAR^e system (Mettler Toledo). The samples were heated from 30 to 500 °C under an inert argon atmosphere. Inductively Coupled Plasma−optical Emission Spectroscopy (ICP − OES) was carried out on an ICPE−9000 spectrometer (Shimadzu) to determine the silicon (Si) content in the electrospun core–shell fibres. Before the analysis, the fibres were hydrothermally digested with nitric acid (65 %, AnalaR NORMAPUR) at 180 °C for 12 h.

2.4. Formulation of the corrosion protective coating

The obtained electrospun nanofibers underwent a resting period at room temperature for 7 days prior to utilization. The direct dispersion of the nanofibers into the coating formulation was not feasible; instead, an additional prior dispersion and drying step were required. Consequently, along with the nanofibers, xylene (Reagent grade, Sigma-Aldrich) was employed at a ratio of 1:10, and stirred overnight at 400 rpm. Subsequent drying under ambient atmospheric conditions at 23 °C for 3 days resulted in the fibres assuming a macroscopic appearance reminiscent of powdered material. The resultant material was then added to a mixture of hydroxyl functional polydimethylsiloxane polymers, namely, WACKER OH − Polymer 1000 and WACKER OH − Polymer 3900 (Wacker Polymers) in xylene, in proportions of 1.0:4.5:1.5; thus, forming component A of the top coat with 3.7 wt% of core–shell fibres. In parallel, TES 40 WN ethyl silicate (Wacker Polymers) and TIBKAT 233 dibutyltin diacetate catalyst (TIB Chemicals) were mixed in xylene (0.25:1.08:1.00), thus forming component B of the

topcoat. Finally, the base component A solution was mixed with the catalyst component B solution in a 3.5:1 ratio.

A stainless steel AISI 304 2B cold laminated plates with 6.0 × 2.5 × 0.1 cm (L × W × H) was employed as the metallic substrate in this study. Before the deposition of the topcoat over the cleaned steel substrate (with acetone), a commercial Hempadur Quattro XO 17870 (Hempel) primer layer was applied, and cured at room temperature for 5 h. The aforementioned topcoat was then applied by the conventional 0.5 mm painting Spray gun. The complete coating was cured for 2 days under ambient conditions.

Four types the specimens were prepared: (*i*) stainless steel (*i.e.*, cleaned metal substrate without any coating); (*ii*) stainless steel + primer coat (final primer thickness of 39 ± 5 μm); (*iii*) control sample consisting of stainless steel + primer coat + top coat without the core–shell fibres (final thickness of 105 ± 19 μm); and (*iv*) self–healing sample consisting of stainless steel + primer coat + self–healing top coat, *i.e.*, top coat containing the electrospun core–shell fibres (final thickness of 174 ± 5 μm).

The final obtained coatings were characterized to determine attributes such as surface, adhesion and mechanical properties. The adhesion was measured by cross-cut tester (Rycobel), based on *ISO 2409: "Paints and varnishes – Cross-cut test"*. Moreover, the mechanical properties were investigated by hardness test using a Buchholz Hardness Tester 3095 (Elcometer), and conducted in accordance with the *ISO 2815: "Paints and varnishes – Buchholz indentation test"*.

2.5. Self–healing and corrosion protection properties

Electrochemical analysis was used to quantify the corrosion protectiveness (*CP*) and the self–healing (*SH*) response. The linear sweep voltammetry (LSV) test was performed by applying a *DC* potential from 0 to 1.2 V using Autolab PGSTAT302N potentiostats/galvanostat (Metrohm) equipped with a FRA32M frequency response analyser (Metrohm) in a three–electrode setup placed inside a Faraday cage. The reference electrode was a silver–silver chloride electrode (Ag/AgCl), while the counter electrode was a platinum wire placed parallel to the coating surface. The working electrode was the test sample, with an exposed area of 2.84 cm^2. The electrolyte was seawater with a pH = 8.2 ± 0.1, salinity of 37.2 psu, and electrical conductivity of 50.9 μS/cm. To induce corrosion response, the samples were mechanically damaged with an *X* − shaped cut of 1 cm^2. After electrochemical testing, optical microscopy was carried out on an Eclipse LV100ND microscope (Nikon) to visualize the evolution of the surface of the damaged area. The *CP* was evaluated by the current density, *J* (mA/cm^2), as a parameter of resistance to the applied potential, *E* (V). The percentage-based total *CP* of the coatings (Eq. (1)) and the *SH* ability (Eq. (2)) of the mechanically–damaged samples were calculated according to the following equations:

$$CP\% = \left(1 - \left(J_{sample}/J_{metal}\right)\right) \times 100 \quad (1)$$

$$SH\% = \left(\left(J_{control} - J_{fibres}\right)/J_{control}\right) \times 100 \quad (2)$$

where J_{sample} stands for the current density of the sample, J_{metal} for the current density of the stainless steel, $J_{control}$ for the current density of the control sample (*i.e.*, topcoat without core–shell fibres), and J_{fibres} for the current density of the self–healing sample (*i.e.*, top coat with core–shell fibres). After the DC voltage variation, an electrochemical impedance spectroscopy (EIS) was also performed. The samples were submitted to a frequency response analyser (FRA) measurement by applying a frequency variation from 10^5 to 10^{-2} Hz with an amplitude omV.

In order to assess the corrosion resistance properties more comprehensively, a Neutral Salt Spray (NSS) test was conducted utilizing a SAL 400-FL Chamber (VLM GmbH), and following the guidelines outlined in the *ISO 9227:2006(E) – Corrosion test in artificial atmospheres – Salt Spray Tests* [37]. Prior to the test, the specimens (in triplicates) were submerged in sea water for 5 min. The coated panels were positioned at a 20° angle to the vertical axis and subjected to continuous spraying for a duration of 240 h (10 days). The outcomes were analysed through visual examination and optical microscopy.

3. Results and discussion

The synthesis of self–healing agent started with the deprotonation of the hydroxyl group of the oleic acid by the trimethylamine, followed by the nucleophilic attack on the chloro(dimethyl)octylsilane and the formation of triethylamine hydrochloride and the intended octyl(dimethyl) silyloleate. The washing process after the reaction was likely to remove the triethylamine hydrochloride precipitates from the solution and after vacuum drying, the final organosilane was obtained. The chemical structure of the as–synthesized material was studied using FTIR, and the collected spectrum mainly presents the peaks related to OH (3741 cm^{-1}) and C—H (2400–3000, 1477 cm^{-1}) groups (Fig. 1). The data also shows intense peaks associated with the desired formation of ester groups, namely, around 1709 and 1200 cm^{-1} from the carbonyl carbon C═O, and at 1172 cm^{-1} from the ester oxygen C—O bonds [38]. In addition, the spectrum shows Si vibration bands at 1396 and 806 cm^{-1}, which are characteristic of Si − CH_2Cl and Si − CH_3 bonds, respectively, as well as a peak at 1034 cm^{-1} associated with Si—O stretches (Fig. 1) [35,39].

After confirming the obtaining of a silyl ester compound, we incorporate the self–healing agent into polymeric PVP solution for coaxial electrospinning alongside polymeric PAN solution, which afforded straightforward access to high–quality silyl ester/PVP@PAN core–shell fibres. The thermal behaviour of the resultant electrospun core–shell fibres, analysed by TGA, revealed that the total weight loss of the core–shell fibres was estimated to be *ca.* 67 %, exhibiting three major weight losses (Fig. 2). The first weight loss was observed between 125 and 280 °C, which is due to the decomposition of silyl ester. Since this compound is decomposed in this temperature range (Fig. 2), it was possible to estimate that the leading of the self–healing agent in the core–shell fibres is *ca.* 3.8 %. Notably, the presence of silyl ester in the electrospun fibres was also confirmed by ICP–OES analysis, which revealed Si content in the core–shell fibres to be 0.0065 mg_{Si}/mg_{fibres}. The second weight loss around 300 °C was associated with the decomposition of the shell PAN polymer, while the third weight loss after 390 °C was attributed to the decomposition of the core PVP polymer, as determined by the TGA analyses of the control hollow PAN fibres (Fig. 2) prepared by coaxial electrospinning without silyl ester/PVP.

TEM was used to gather information about the microstructure, size,

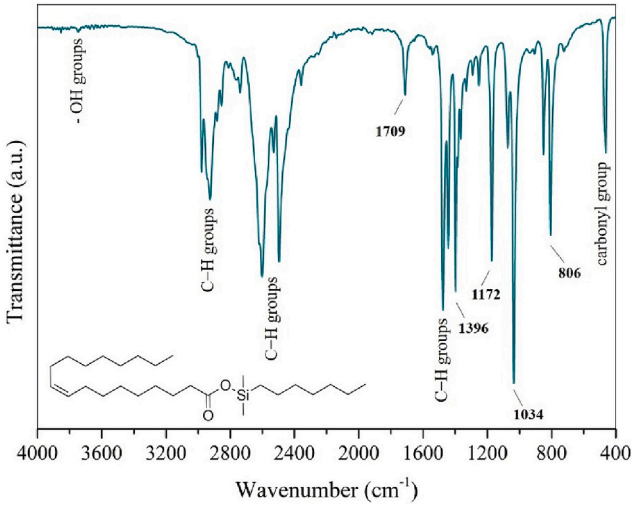

Fig. 1. FTIR spectrum of the synthesized silyl ester, together with the inset showing its chemical structure.

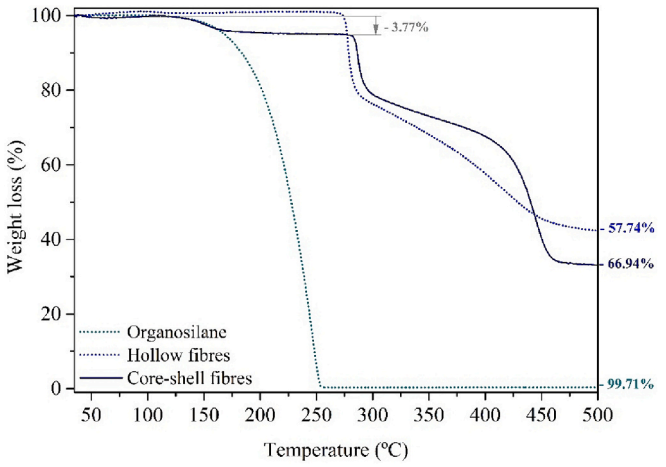

Fig. 2. TGA profiles of the synthesized silyl ester and electrospun fibres (see Appendix for the derivative curves).

and shape of the self–healing agent, as well as electrospun products. Fig. 3a shows a low-magnification TEM image of the synthesized silyl ester, which exhibits an amorphous–like appearance with an average particle size of about 170 ± 23 nm. The microstructure of the electrospun silyl ester/PVP@PAN core–shell fibre is shown in Fig. 3c-d, while Fig. 3b demonstrates a low–magnification TEM image of the control hollow PAN fibre, electrospun without silyl ester/PVP. In the core–shell system, it is possible to observe that the silyl ester/PVP core is slightly darker than the PAN shell which presented a thickness of about 21 ± 4 nm. At higher magnification, the nanoparticles of silyl ester are visible inside the electrospun material (Fig. 3d). Hence, the TEM results suggest that the core of the fibres consists of a silyl ester self–healing agent well–dispersed within the PVP matrix, and this silyl ester/PVP core is well–covered by a thin shell of PAN polymer.

The nanofibers diameters were obtained through analysis of 50 measurements derived from the SEM image of intact silyl ester/PVP@PAN core-shell fibres (Fig. 4a). The mean diameter was 502 nm, exhibiting a standard deviation of 155 nm. We next probed the morphological and chemical evolutions of the electrospun silyl ester/PVP@PAN core–shell fibres, as a consequence of the moisture–assisted hydrolysis of 3.7 % silyl ester compound encapsulated within the fibres. For this purpose, a piece of the fibre was placed onto carbon tape, and then several cuts were performed. Afterwards, the piece was exposed to water for a couple of minutes, dried under ambient conditions, and visualized by SEM. The control intact fibres (Fig. 4a) exhibit a random arrangement with expected tubular–like shape, without the presence of any beads or defects. In sharp contrast, a dense mass around fibres (Fig. 4b) and the appearance of the agglomerates (Fig. 4b, arrows) are observed for mechanically–damaged silyl ester/PVP@PAN core–shell fibres after their exposure to water.

From the SEM results, it could be deduced that after the mechanical rupture of the thin PAN shell and subsequent exposure of the contained silyl ester to the moisture, the hydrolysis of the organosilane compound occurs, forming a silanol product alongside an oily layer. This deduction was further supported by the FTIR analysis of the intact and mechanically damaged specimens (Fig. 5). Specifically, alterations were observed in the peaks related to the ester groups around 1716–1731 cm^{-1}, while the bands related to free OH groups at 3853–3746 cm^{-1} were not observed on the damaged core–shell fibres. The bands observed at 1672 and 1446 cm^{-1} were addressed to the absorbed water on the Si–OH hydrolysis product [40], and at 1289 cm^{-1} was attributed to Si − CH_3 bonds. The characteristic peaks of Si—O stretches were detected at 1068 and 1037 cm^{-1} [35], while the peak at 534 cm^{-1} was most likely associated with chlorosilane compound [39], maybe remnants from the silyl ester synthesis.

With these mechanistic insights, we hypothesize that our novel silyl ester/PVP@PAN core–shell product with 3.7 % loading of silyl ester could provide an efficient self–healing functionality to the corrosion protective coatings. To verify the hypothesis, we formulate two–component coating for steel protection while incorporating our electrospun core–shell fibres. This new coating formulation was then applied to steel substrates by conventional Spray–painting, and the resultant specimens, alongside control specimens, underwent some characterization technique and electrochemical testing. Cross-cut evaluations in all the samples revealed minor flake detachment at intersections, indicative of robust adhesion classified at the second highest level on a 6-grade scale, affecting less than 5 % of the total area. Buchholz hardness tests, quantified in BH values, demonstrated that the inclusion of nanofibers led to a minor reduction in hardness by approximately 5 % (70 ± 3 BH, control samples and 66 ± 6 BH, self-healing top-coated samples). However, these values remained higher compared to coatings with primer alone (52 ± 2 BH). Overall, the characterization highlighted the coatings' suitability for corrosion protection evaluation, with no apparent compromise in performance.

To evaluate the corrosion protection behaviour and the self–healing response of the novel coating, cathodic protection current density, *J*, was monitored as a function of the applied potential, *E*. In general, *J* increases if the coating has a defective area(s) where the electrolyte can penetrate to the metallic substrate underneath the protective coating, or if the metallic substrate is simply non–coated [15,41].

Fig. 6a summarizes the results of the *J*(*E*) electrochemical testing. An intact protective coating has a near to zero *J*(*E*) response even under high applied *E*, showing a corrosion protectiveness *CP* = 100 % (Fig. 6a, blue *J*(*E*) curve). The first control specimen of stainless steel exhibits the highest *J*, and accordingly *CP* = 0 % (Fig. 6a, black *J*(*E*) curve). The second control specimen of steel + primer coat was found to exhibit *CP* = 34 % (Fig. 6a, green *J*(*E*) curve). For the third control specimen of stainless steel + primer coat + topcoat, the average current density was measured to be 1.17 mA/cm^2, resulting in *CP* = 57 % (Fig. 6a, cyan *J*(*E*) curve). The data shows that the addition of a topcoat to the steel + primer coat system leads to an improvement in corrosion protection response by 23 %. The specimens of steel + primer coat + self–healing topcoat containing our novel electrospun silyl ester/PVP@PAN core–shell fibres, reveals excellent corrosion protective properties of the newly developed formulation, as manifested by the measured average *J* of only 0.029 mA/cm^2 and *CP* = 98.9 % (Fig. 6a, pink *J*(*E*) curve). Furthermore, this specimen was left immersed in the electrolyte solution (*i.e.*, in seawater) for 24 h to evaluate the impact of the time on the corrosion protective properties. The final *J* was measured to be of only 0.096 mA/cm^2 with *CP* = 96.4 % (Fig. 6a, dark red *J*(*E*) curve), evidencing stable performance of the coating against the corrosion. The self–healing (*SH*) response of newly developed coating was quantified by contrasting the results measured for the control steel + primer coat + topcoat and the targeted steel + primer coat + self–healing topcoat specimens. This comparison shows that our novel coating for corrosion protection of steel exhibits an immediate self–healing capability of *SH* = 97.5 %, which slightly decreases to *SH* = 91.8 % after 24 h in seawater.

The Bode Plot (impedance modulus, |Z| × frequency) is presented in Fig. 6b. The higher the impedance modulus the higher is the barrier of protection. As expected, the original metal had the lowest modulus, and the intact control and the intact SH coating samples presented similar higher results, indicating that the presence of the nanofibers did not significantly affect the resistance of the initial coatings. The damaged samples with steel + primer coat and the damaged controls (steel + primer coat + top coat without healing agent) had a steady |Z| at the order on 10^3 Ω cm^2 even with the frequency variation. The damaged SH coatings (stainless steel + primer coat + top coat with healing agent) presented better results than the control ones, being that the samples immersed for 24 h had a good response, but lower values than the intact ones, with the increase of the impedance modulus inversely proportional to the frequency decrease. The SH coating immediately tested,

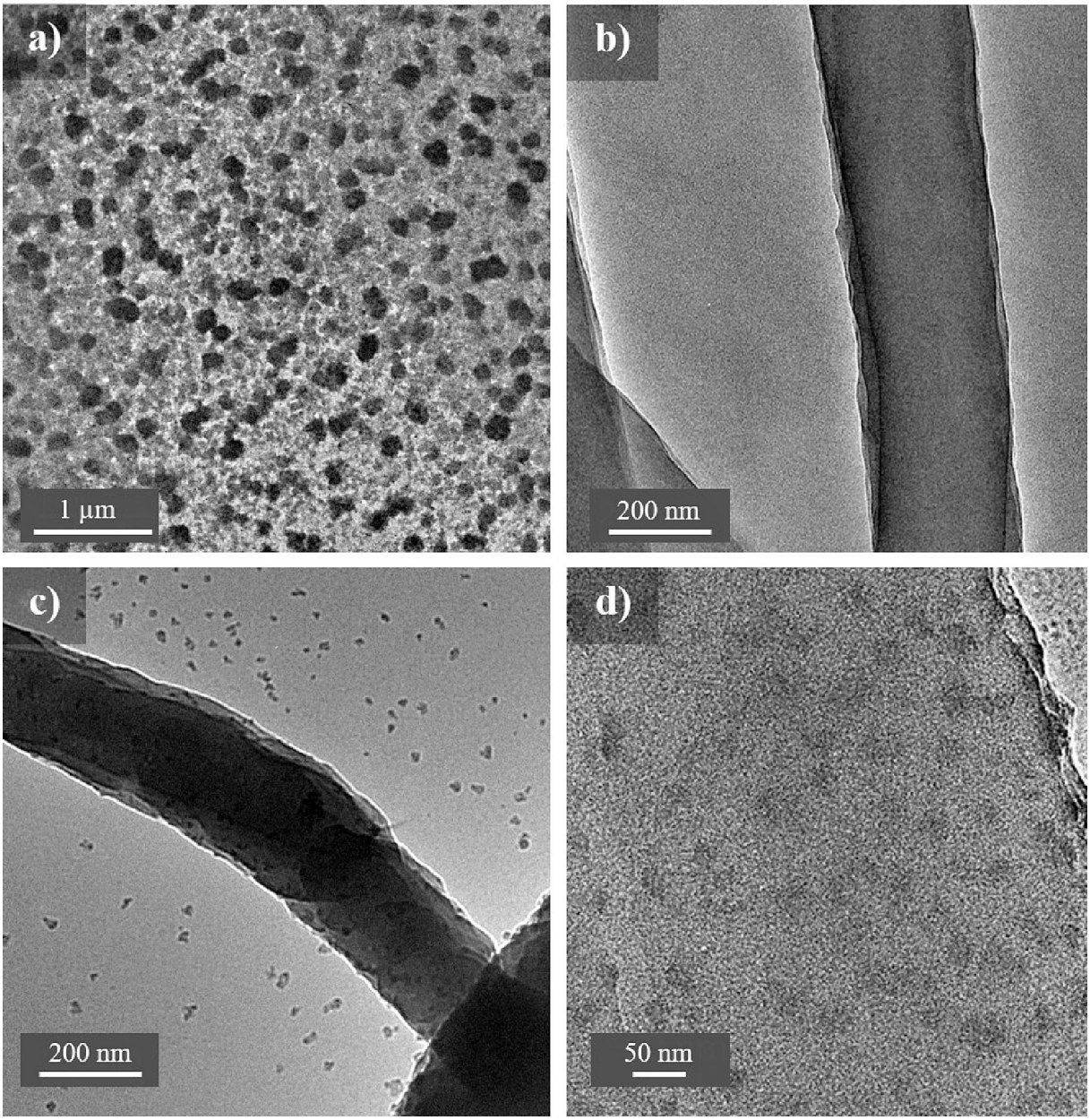

Fig. 3. Representative TEM images of a) synthesized silyl ester, b) control electrospun hollow PAN fibre, and c) and d) targeted electrospun silyl ester/PVP@PAN core–shell fibre.

had a steady |Z| at the order on 10^4 Ω cm^2 with the frequency variation. The highest values between the damaged primer, the damaged control and the damaged metal samples.

The differences in the electrochemical behaviour of the samples can also be observed in the Nyquist Plots of the coated substrates (Fig. 6c). The intact coating curve lacked a semi-circular appearance, instead displaying a straight line proximate to the imaginary axis, signifying a high impedance response dominated by a capacitance element [42]. The damaged SH coating revealed a well–defined capacitance arc in the high-frequency range signifying the prevalence of a capacitive behaviour [43]. However, following a 24 h immersion, the damaged SH coatings manifested a 45° line at high frequencies, indicative of a Warburg-like response associated with porous surfaces [44]. Concurrently, the damaged control coating exhibited a reduced semicircle radius, suggesting diminished coating resistance and heightened electrolyte permeation [45,46].

To a deeper comprehension of the electrochemical dynamics and corrosion resistance intrinsic to the coating, the impedance results were subjected to an equivalent circuit fitting assisted by the Metrohm NOVA® 2.1 software. The simulation points from the fitting process are represented in Fig. 6c – continuous line. The model selected precisely matched the experimental data acquired from the as-prepared samples. The circuit comprises of a series arrangement of a resistor and a parallel configuration involving a constant phase element and a resistor in series with another constant phase element in parallel to another resistor, [R(Q[R(QR)])] (Fig. 6c). This model is considerate an effective route to simulate and interpret impedance results of steel corrosion [42,47]. R_s is the solution resistance, C_c is the constant phase element that represents the capacitive behaviour of the coating film, R_c the resistance of the coating, and C_{dl} corresponds to the localized double-layer capacitance, and R_{ct} stands for the charge transfer resistance. Table 1 delineates the capacitance and resistance parameters of the formulated coatings, specifically associated with the first time constant, serving as a representative measure of the electrical and barrier characteristics of this layer

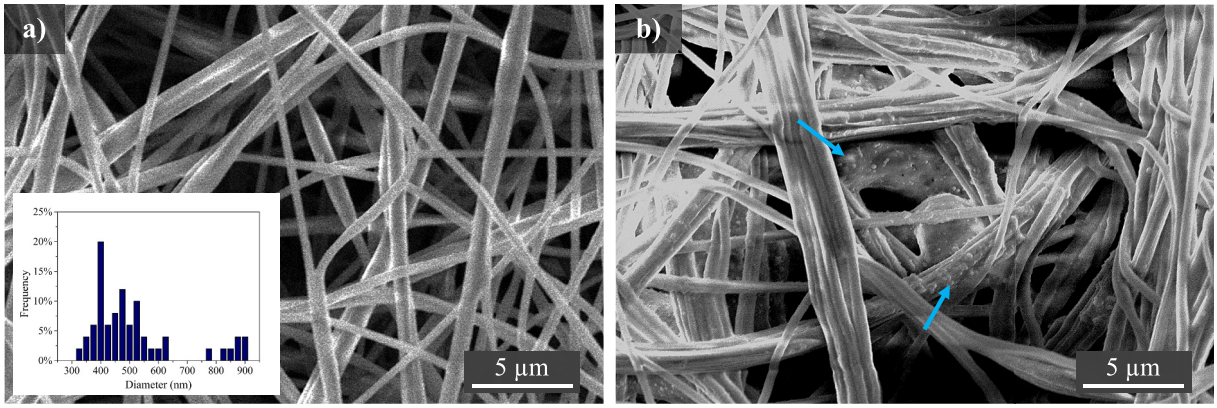

Fig. 4. Microstructure, size, and shape of the nanofibers, a) SEM image of the control intact, and fibres diameter distribution, in nm, and b) SEM image of the mechanically–damaged silyl ester/PVP@PAN core–shell fibres after their subsequent exposure to moisture.

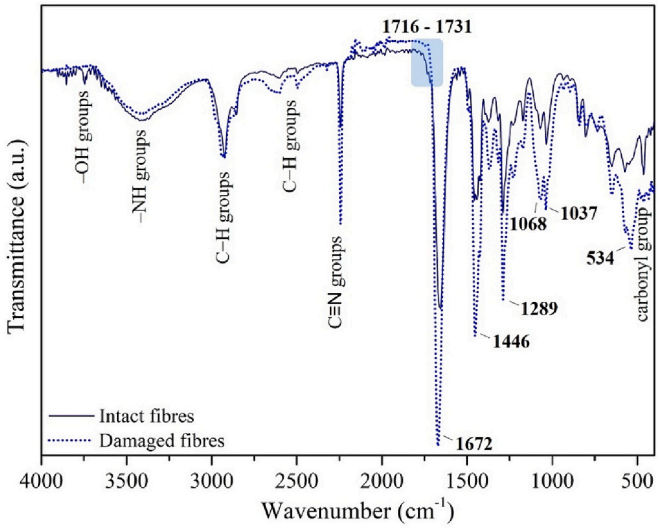

Fig. 5. Comparison of the FTIR spectra of the control intact and mechanically–damaged silyl ester/PVP@PAN core–shell fibres after their subsequent exposure to moisture.

[48]. In the case of the intact coating, the resistance (R_c) was in the order of 10^6 Ω cm^2, 10^4 Ω cm^2 for the both conditions of the damaged SH coatings, and 10^3 Ω cm^2 for the damaged control. Following damage, the SH coating demonstrated the lowest capacitance value among all specimens ($C_c = 3.4 \times 10^{-5}$ µS/cm^2 s^n), surpassing even the intact coatings (1.3×10^{-4} µS/cm^2 s^n). This reaffirms the outstanding insulating properties and prompt self-healing response exhibited by the SH coatings. As indicated by a high capacitance exponent ($n = 0.92$, for the intact coating and $n = 1.00$ for the damaged SH coating), these both coatings presented a capacitive behaviour [49]. Concerning the SH coating subjected to a 24 h immersion post-damage, it exhibited a diminished C_c values compared to the immediately immersed damaged coatings, with a corresponding $n = 0.57$, confirming the suggested presence of a Warburg impedance element behaviour. [47]. As the electrolyte solution systematically permeates the coating, there is a simultaneous reduction in coating resistance accompanied by an augmentation in coating capacitance. This precise scenario is exemplified by the damaged control ($C_c = 2.5 \times 10^{-3}$ µS/cm^2 s^n and $n = 0.72$).

In this context, in addition to alterations in coating resistance and capacitance, the fluctuations observed in phase angles (Fig. 6d) also indicates of the performance of coatings. The analysed samples predominantly exhibited a capacitive response across the entire frequency spectrum. The intact coating presented a wide frequency range around −90°, indicating the strong corrosion resistance of the initial layer [45,50]. The damaged SH coating and damaged control presented initial values higher than −40°. Upon saturation of electrolyte permeation into the surface of the coating, the capacitance stabilizes and the resistance decreases, resulting in a swift reduction in the phase angles, particularly evident in high-frequency [42,51]. Within the mid-frequency range (1 to 100 Hz), a resistive response was observed, indicating favouring current passage through the resistor [45]. A new peak appeared close to the 0.1 Hz denoting the presence of a second time constant [52], with higher angles observed for both intact and damaged SH coatings. At low frequencies, the damaged control (top coating with the self-healing agent) curve decreased quickly with the decrease of coating resistance, once the current flowing through gradually increase. The resistive region at low frequencies indicated electrolyte diffusion and a consequent loss of adhesion at the interface with the substrate due to some corrosion reactions taking place [45]. Notably, there was a diverged behaviour for the damaged SH coating after 24 h of immersion. Herein, with the presence of a Warburg element, it exhibited the maximum phase angle near the frequency of 1 Hz, and lower values in both higher and lower frequencies. The discrete appearance of the two time constant peaks (around 10^3 and 1 Hz) was challenging to distinguish. Due to the time immersed, the permeation process could have stabilized by the time that the test started, however, the phase angle distant from 0° suggested the existence of a protective layer, contributing to a corrosion-resistant barrier.

From EIS it is also possible to semi−quantify the protective behaviour of the coatings. The impedance modulus at low frequencies such as 0.01 [53–55] and 0.1 Hz [56,57] is often used as indicative of corrosion resistance. Table 2 presents the mean values obtained from the sample tests. Once again, higher values of the impedance modulus denote higher barrier properties and protection. The intact complete coatings (control and SH coating) presented impedance modulus in the order of 10^9 and 10^{10} Ω cm^2 in the relevant frequency. The damaged control samples had values of 10^2 and 10^3 Ω cm^2 and the damaged SH coatings |Z| were 10^5 Ω cm^2 for the immediate tests and 10^8 and 10^7 Ω cm^2 after 24 h of immersion. These results corroborate with the ones obtained in the $J(E)$ analysis. Thus, it was possible to observe that the incorporation of novel electrospun core–shell fibres into an advanced coating formulation affords an efficient self–healing functionality to the resultant corrosion protective coating.

The electrochemically tested specimens were also inspected by optical microscopy. Expectedly, (intense) pitting corrosion was visualized in the case of all control specimens without self–healing capability: stainless steel (Fig. 7a), steel + primer coat (Fig. 7b), and steel + primer coat + topcoat (Fig. 7c). Completely different behaviour was observed for the newly developed coating containing core–shell fibres, which provide the self–healing capability. Specifically, one could see that the

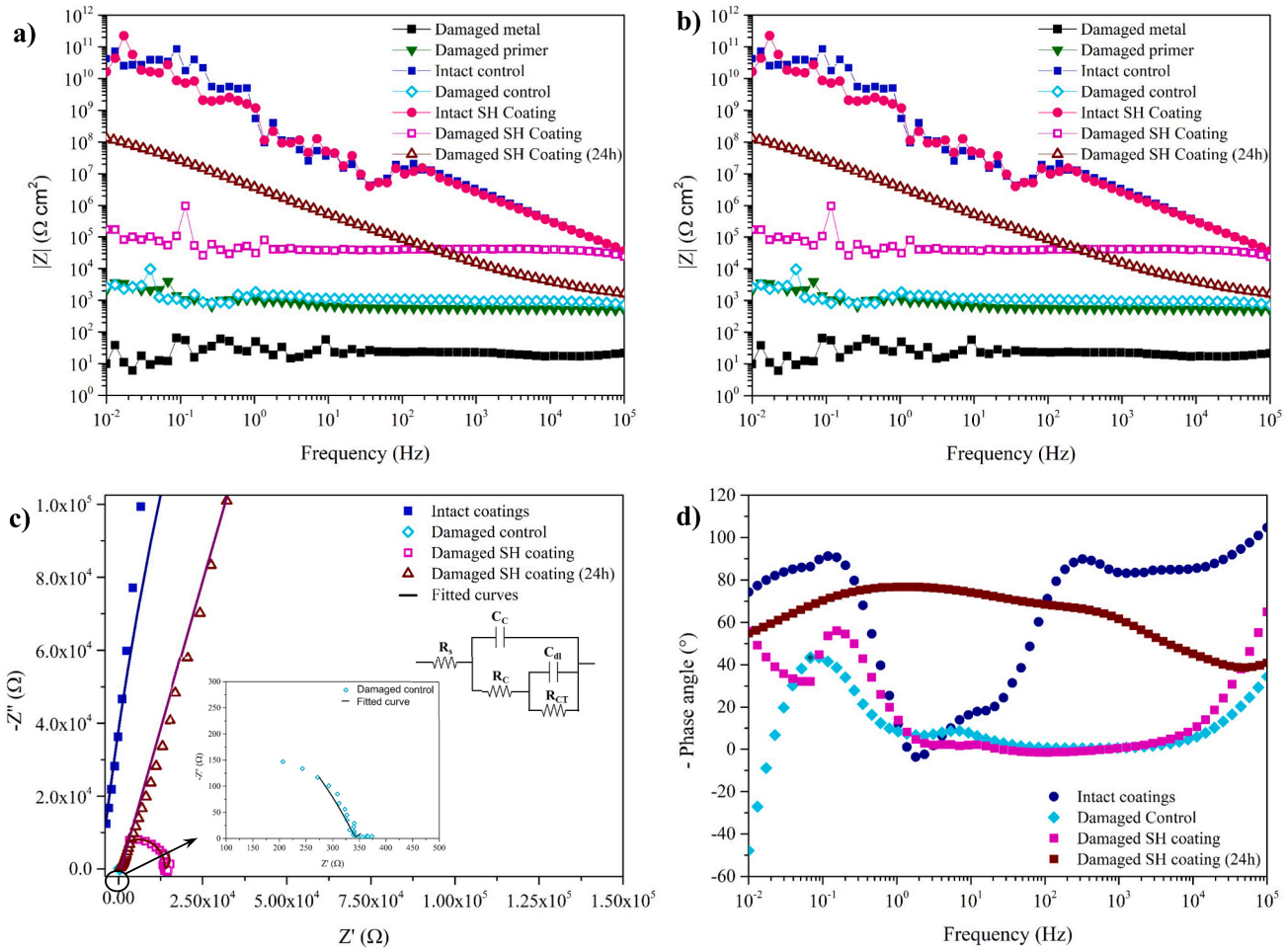

Fig. 6. Electrochemical analysis, recorded at room temperature after mechanical damage with an *X*−shaped cut of 1 cm^2 using seawater as an electrolyte, a) *J(E)* dependence data for the different specimens, b) Bode Plot, c) enlarged view of high frequency response on Nyquist plot and equivalent circuit fitting curves for the coated samples, and d) phase angle plot for the coated samples.

Table 1
Coatings' capacitance and resistance parameters obtained through its equivalent circuit fitting.

Samples	C_c		R_c
	Y_o (μS/cm^2 s^n)	n	(Ω cm^2)
Intact coating	1.3×10^{-4}	0.92	5.7×10^6
Damaged control	2.5×10^{-3}	0.72	4.0×10^3
Damaged SH coating	3.4×10^{-5}	1.00	4.4×10^4
Damaged SH coating after 24 h immersion	3.5×10^{-3}	0.57	1.5×10^4

Table 2
Impedance modulus at low frequencies as an indicative of corrosion resistance.

Samples	$\|Z\|_{0.01\ Hz}$ (Ω cm^2)		$\|Z\|_{0.1\ Hz}$ (Ω cm^2)	
Damaged metal	1.0×10^1	$\pm 5.3 \times 10^1$	5.6×10^1	$\pm 3.9 \times 10^1$
Damaged primer	2.0×10^3	$\pm 2.3 \times 10^4$	1.1×10^3	$\pm 3.6 \times 10^4$
Intact control sample	4.3×10^{10}	$\pm 4.7 \times 10^{10}$	1.8×10^{10}	$\pm 1.0 \times 10^{10}$
Damaged control	2.6×10^3	$\pm 1.6 \times 10^3$	8.1×10^2	$\pm 3.3 \times 10^3$
Intact SH coatin	1.6×10^{10}	$\pm 5.0 \times 10^{10}$	7.2×10^9	$\pm 9.7 \times 10^9$
Damaged SH coating	1.7×10^5	$\pm 8.0 \times 10^7$	9.7×10^5	$\pm 1.1 \times 10^8$
Damaged SH coating after 24 h immersion	1.3×10^8	$\pm 2.3 \times 10^8$	2.7×10^7	$\pm 4.0 \times 10^7$

mechanical damage with an *X* − shaped cut is entirely healed (Fig. 7d), thus preventing the corrosion of the steel substrate during the electrochemical testing. Notably, only the coating containing silyl ester/PVP@PAN core–shell fibres fully protected steel against corrosion (Fig. 7d).

The NSS test served as an additional evaluation tool to assess the corrosion resistance of the materials under investigation (Fig. 8). By subjecting the specimens to a controlled corrosive environment, the test facilitated the observation of potential weaknesses and vulnerabilities in the coatings protectiveness. The corrosion observed was comparatively lower than the one induced in the electrochemical tests; nevertheless, discernible differences were still evident. Both metal and primer samples (Fig. 8a-b), exhibited a distinct brownish discoloration around the artificial damaged area. Controls specimens (Fig. 8c) displayed a more subtle manifestation of such discoloration, yet signs of corrosion were still perceptible. In stark contrast, the self-healing developed coating (Fig. 8d), revealed an absence of exposure and corrosion of the metal upon microscopic examination following the salt exposure. These findings underscore the valuable results garnered, demonstrating the durability and performance of coatings containing self-healing agents when

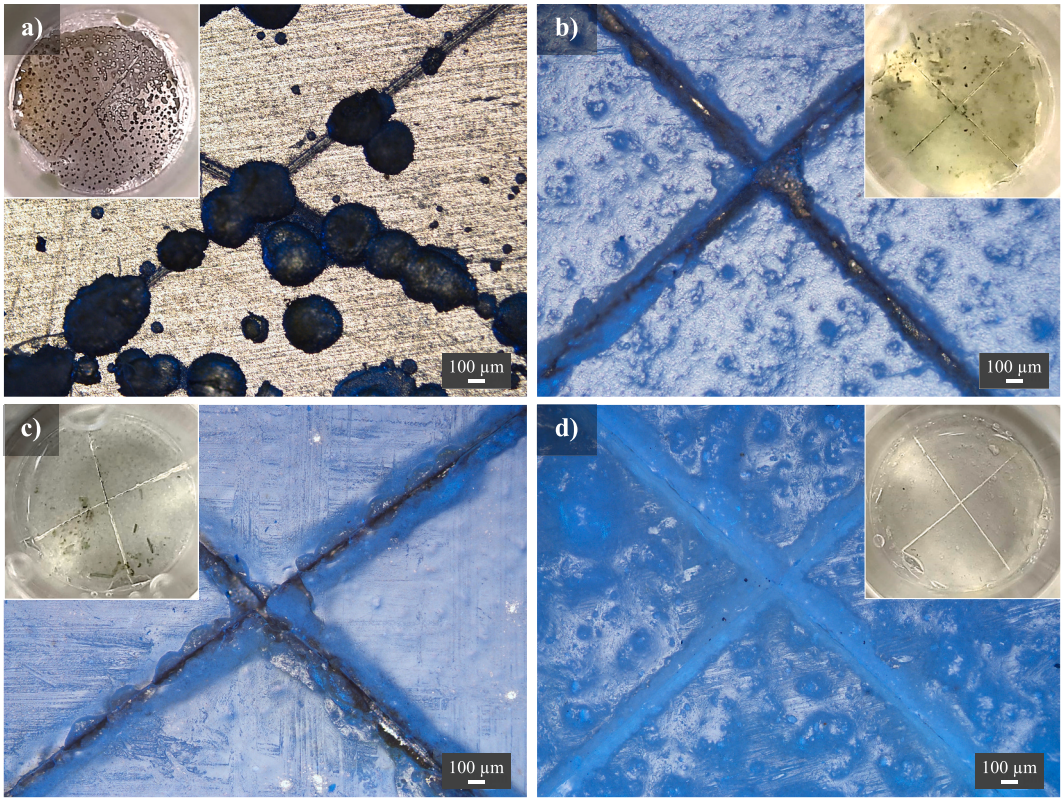

Fig. 7. Optical microscopy images and digital photographs (insets) of the electrochemically–tested specimens: a) stainless steel, b) steel + primer coat, c) steel + primer coat + topcoat, and d) steel + primer coat + self–healing topcoat. Note the absence of corrosion in d) for newly developed coating with the self–healing capability.

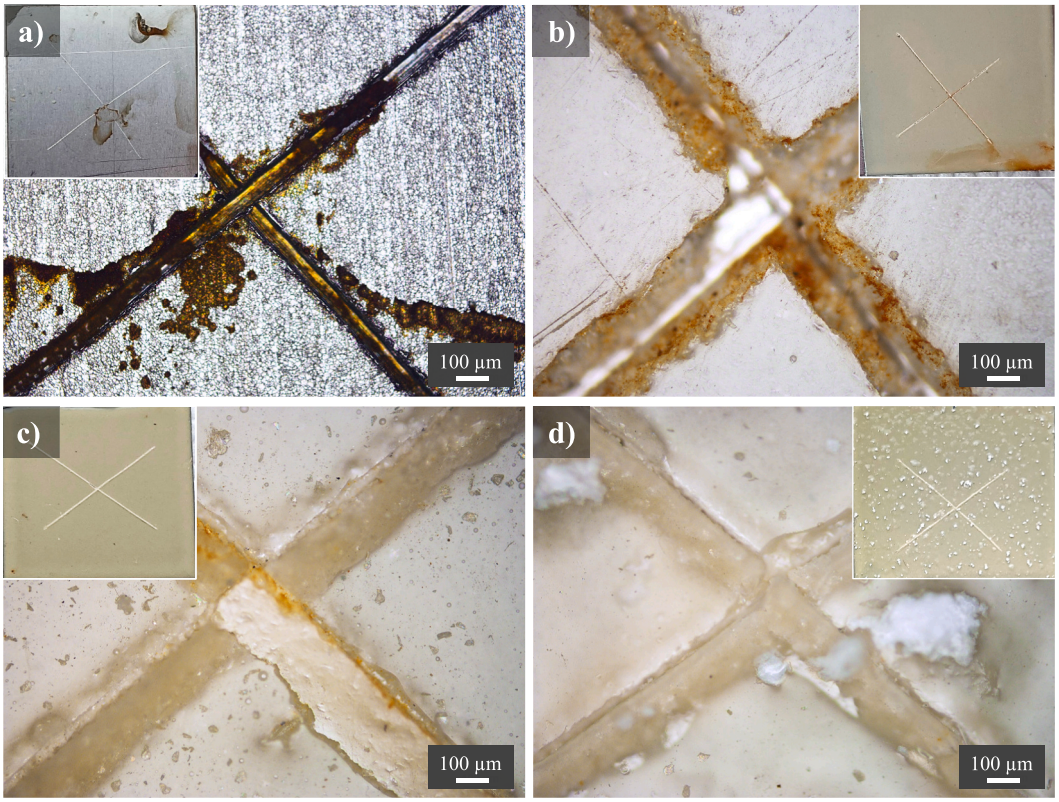

Fig. 8. Optical microscopy images and digital photographs (insets) of the NSS–tested specimens after 240 h: a) stainless steel, b) steel + primer coat, c) steel + primer coat + topcoat, and d) steel + primer coat + self–healing topcoat. Note the absence of corrosion in the newly the developed coating with the self–healing capability.

subjected to challenging environmental conditions, particularly those simulating saline atmospheres.

3.1. Self-healing mechanism

An efficient corrosion protective coating with self–healing capability can be obtained in three steps: (*i*) synthesis of a silyl ester–based compound, which undergoes hydrolysis in the presence of moisture acting as self–healing agent; (*ii*) coaxial electrospinning of silyl ester/PVP@PAN core–shell fibres, wherein the silyl ester self–healing agent is well–distributed within polymeric PVP core while being simultaneously well–protected from moisture by polymeric PAN shell; and (*iii*) formulation of novel corrosion protection coating based on polydimethylsiloxane polymers and the electrospun core–shell fibres, and Spray-painting application.

Although the reported literature has evidenced that organosilane compounds are good candidates for self–healing functional coatings, interestingly, this was only realized in capsule–like systems [11,31,58]. In this work, to the best of our knowledge, we were able for the first time to incorporate an organosilane self–healing agent into core–shell fibres using a coaxial electrospinning technique. The main challenge here is the lack of the possibility for direct electrospinning of organosilane compounds due to their low electrical conductivity, which was successfully overcame by mixing silyl ester self–healing agent with a well–electrospinnable PVP polymer [59,60].

The corrosion protectiveness ability of the newly developed coating was quantified to be outstanding with *CP* value of 98.9 %. The self–healing mechanism of the coating is schematically proposed in Fig. 9. Once the polymeric PAN shell of silyl ester/PVP@PAN core–shell fibres is disrupted, the silyl ester/PVP core is exposed to ambient conditions, and the silicon–oxygen (Si − O) bonds of silyl ester react with the water molecule, thus splitting into a silanol and fatty oleic acid. Further, the resultant groups from hydrolysis undergo a condensation that gives a crosslinked structure. Both silica and oleic acid products then heal the mechanical damage while adhering to the steel, thus preventing the corrosive environment from getting in contact with the substrate. Notably, the use of this specific silyl ester organosilane is beneficial because the fatty oleate groups attached to the silane additionally protect this compound from unwanted reactions before mechanical damage [33].

After the damage of the coating, an excellent immediate healing response of *SH* = 97.5 % was observed, which highlights that our newly developed coating is capable of rapidly protecting the steel from corrosion. In the literature, Garcia et al. [35] achieved a plateau of self–healing response at *SH* = 75 % by applying the same type of organosilane in the core of poly(urea–formaldehyde) microcapsules. In another work, the same shell material, prepared by *in situ* polymerization, encapsulated fluorinated alkyl silane as the repairing agent in the core, which resulted in 64.5 % of the initial impedance modulus, greater than the one obtained with the control coating [54]. Using the nanofibers approach, Doan et al. [25] achieved 88 % corrosion inhibition efficiency with two complementary fibres, namely, one with poly(dimethylsiloxane) and poly(diethoxysiloxane), and another one with a curing agent. The electrospun fibres were deposited directly onto the substrate, alternating layer by layer of each fibre type, by intervals of 1 h, resulting in four final layers subsequently spun cast with a silicone binder to obtain the composite coating. Ji et al. [27] obtained *SH* efficiencies of 95.96 % in alkaline media with core−shell electrospun pH–responsive fibres. The shell was based in cellulose acetate and the core was loaded with oleic acid and alkyd varnish resin. The final coating was obtained by spin coating PDMS into the fibre's membranes. With another strategy, Cao et al. [61] were able to achieve a 98.4 % cure rate in a damaged area with one–component fibres. The nanofibers with 1,10–phenanthroline core and poly(vinyl alcohol)/chitosan shell were directly electrospun into the metal substrate, and posteriorly spin-coated with epoxy resin and polyamide. In our approach, the core–shell nanofibers were detached from the aluminium foil collector after the coaxial electrospinning and dispersed in a liquid coating formulation to be applied to the metallic substrate by a conventional one–step spraying technique, which is compatible and favourable with the application and maintenance of offshore structures.

4. Conclusions

Self–healing materials are a promising technology for protective coatings due to their distinguished ability to recover their properties and functionality after damage. Unlike the costly conventional approaches that use a two−component healing agent, here it was demonstrated a potential single−component healing agent, synthesized and incorporated in the core of core–shell nanofibers. The self–healing material was shown to be water−reactive once damage occurs and the shell is disrupted. The dispersion of the nanofibers resulted in a powder−like material and it was successfully applied in a solvent−based formulation (due to the reactivity of the healing agent to water). The limitations of up-scaling processes for self-healing coating technologies were overcome by implementing a viable coating technique that is already widely applied in large-scale structures – Spray painting. The metallic substrates were coated combining a 2 − layer coating (primer and top coating). After exposure to a corrosive environment and testing for corrosion induction in electrochemical tests, the coatings containing the nanofibers presented an excellent immediate healing response of SH = 97.5 %. All the coated samples impedance data were fitted to an equivalent circuit and the self-healing coatings exhibited the lowest capacitance values, suggesting a robust protective barrier. The neutral

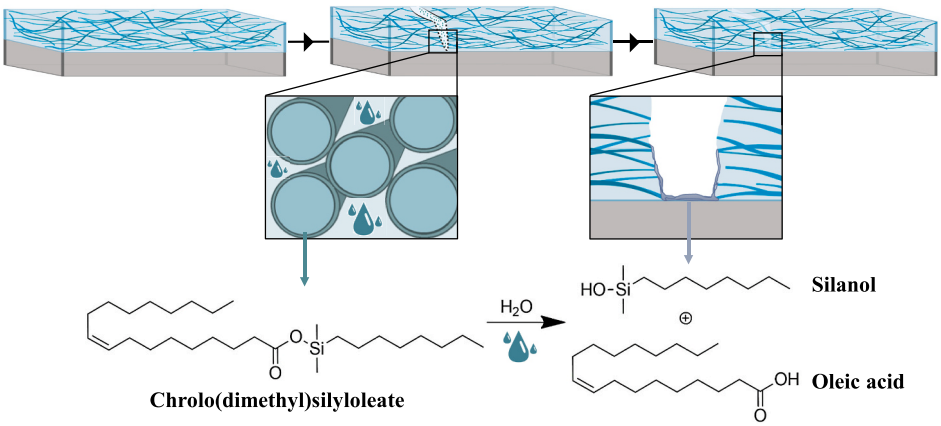

Fig. 9. The proposed mechanism for the self–healing of the coating after mechanical damage.

salt pray test also highlighted that our newly developed coating is capable of rapidly protecting the steel from corrosion as a catalyst–free "autonomous" self–healing mechanism.

CRediT authorship contribution statement

Natalia C.M. Spera: Writing – original draft, Visualization, Validation, Methodology, Investigation, Data curation, Conceptualization. **Cristina Salazar-Castro:** Writing – review & editing, Conceptualization. **Paula C. Álvarez de Eulate:** Writing – review & editing, Conceptualization. **Yury V. Kolen'ko:** Writing – review & editing, Validation, Project administration, Funding acquisition. **Juliana P.S. Sousa:** Writing – review & editing, Validation, Supervision, Project administration, Methodology, Funding acquisition, Conceptualization.

Declaration of competing interest

The authors declare that they have no known competing financial interests or personal relationships that could have appeared to influence the work reported in this paper.

Data availability

The data that has been used is confidential.

Acknowledgement

This work was supported by the European Union's Horizon 2020 research and innovation program under Grand Agreement N° 952960.

Appendix A

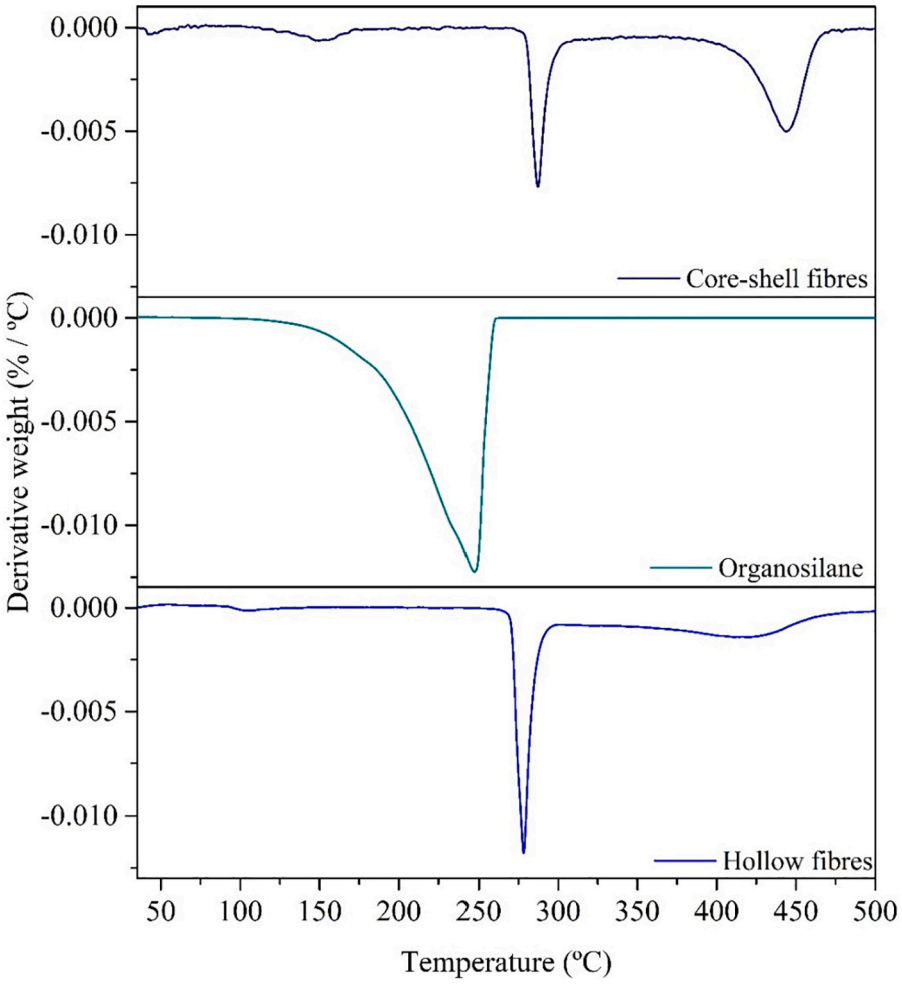

Fig. A.1. TGA derivatives of the core–shell fibres, silyl ester and hollow PAN fibres.

References

[1] G. Koch, J. Varney, N. Thompson, O. Moghissi, M. Gould, J. Payer, International measures of prevention, application, and economics of corrosion technologies study, NACE-Int. Corros. Conf. Ser. (2016) 216.
[2] G.W. Goward, Protective coatings – purpose, role, and design, Mater. Sci. Technol. 2 (1986) 194–200, https://doi.org/10.1179/mst.1986.2.3.194.
[3] A.A. Olajire, Recent advances on organic coating system technologies for corrosion protection of offshore metallic structures, J. Mol. Liq. 269 (2018) 572–606, https://doi.org/10.1016/j.molliq.2018.08.053.
[4] A. López-Ortega, R. Bayón, J.L. Arana, Evaluation of protective coatings for high-corrosivity category atmospheres in offshore applications, Materials (Basel) 12 (2019) 1325, https://doi.org/10.3390/ma12081325.
[5] M.I. Blanco, The economics of wind energy, Renew. Sust. Energ. Rev. 13 (2009) 1372–1382, https://doi.org/10.1016/j.rser.2008.09.004.

[6] S.J. Price, R.B. Figueira, Corrosion protection systems and fatigue corrosion in offshore wind structures: current status and future perspectives, Coatings 7 (2017) 25, https://doi.org/10.3390/coatings 7020025.
[7] M.F. Montemor, Functional and smart coatings for corrosion protection: a review of recent advances, Surf. Coat. Technol. 258 (2014) 17–37, https://doi.org/10.1016/j.surfcoat.2014.06.031.
[8] A. Kumar, L.D. Stephenson, J.N. Murray, Self-healing coatings for steel, Prog. Org. Coat. 55 (2006) 244–253, https://doi.org/10.1016/j.porgcoat.2005.11.010.
[9] A. Stankiewicz, I. Szczygieł, B. Szczygieł, Self-healing coatings in anti-corrosion applications, J. Mater. Sci. 48 (2013) 8041–8051, https://doi.org/10.1007/s10853-013-7616-y.
[10] B.J. Blaiszik, S.L.B. Kramer, S.C. Olugebefola, J.S. Moore, N.R. Sottos, S.R. White, Self-healing polymers and composites, Annu. Rev. Mater. Res. 40 (2010) 179–211, https://doi.org/10.1146/annurev-matsci-070909-104532.
[11] M. AbdolahZadeh, S. Van Der Zwaag, S.J. Garcia, Self-healing corrosion-protective sol-gel coatings based on extrinsic and intrinsic healing approaches, in: M. D. Hager, S. Van Der Zwaag, U.S. Schubert (Eds.), Self-Healing Mater, 1st ed, Springer, Cham, Switzerland, 2016, pp. 185–218, https://doi.org/10.1007/12_2015_339.
[12] B.J. Blaiszik, M.M. Caruso, D.A. McIlroy, J.S. Moore, S.R. White, N.R. Sottos, Microcapsules filled with reactive solutions for self-healing materials, Polymer (Guildf) 50 (2009) 990–997, https://doi.org/10.1016/j.polymer.2008.12.040.
[13] B.J. Blaiszik, N.R. Sottos, S.R. White, Nanocapsules for self-healing materials, Compos. Sci. Technol. 68 (2008) 978–986, https://doi.org/10.1016/j.compscitech.2007.07.021.
[14] V.K. Thakur, M.R. Kessler, Self-healing polymer nanocomposite materials: a review, Polymer (Guildf) 69 (2015) 369–383, https://doi.org/10.1016/j.polymer.2015.04.086.
[15] V. Sauvant-Moynot, S. Gonzalez, J. Kittel, Self-healing coatings: an alternative route for anticorrosion protection, Prog. Org. Coat. 63 (2008) 307–315, https://doi.org/10.1016/j.porgcoat. 2008.03.004.
[16] D.G. Bekas, K. Tsirka, D. Baltzis, A.S. Paipetis, Self-healing materials: a review of advances in materials, evaluation, characterization and monitoring techniques, Compos. Part B 87 (2016) 92–119, https://doi.org/10.1016/j.compositesb.2015.09.057.
[17] S. An, M.W. Lee, A.L. Yarin, S.S. Yoon, A review on corrosion-protective extrinsic self-healing: comparison of microcapsule-based systems and those based on core-shell vascular networks, Chem. Eng. J. 344 (2018) 206–220, https://doi.org/10.1016/j.cej.2018.03.040.
[18] C.J. Hansen, W. Wu, K.S. Toohey, N.R. Sottos, S.R. White, J.A. Lewis, Self-healing materials with interpenetrating microvascular networks, Adv. Mater. 21 (2009) 4143–4147, https://doi.org/10.1002/adma.200900588.
[19] S. An, M. Liou, K.Y. Song, H.S. Jo, M.W. Lee, S.S. Al-Deyab, A.L. Yarin, S.S. Yoon, Highly flexible transparent self-healing composite based on electrospun core-shell nanofibers produced by coaxial electrospinning for anti-corrosion and electrical insulation, Nanoscale 7 (2015) 17778–17785, https://doi.org/10.1039/c5nr04551g.
[20] J.H. Park, P.V. Braun, Coaxial electrospinning of self-healing coatings, Adv. Mater. 22 (2010) 496–499, https://doi.org/10.1002/adma.200902465.
[21] S. Sinha-Ray, D.D. Pelot, Z.P. Zhou, A. Rahman, X.F. Wu, A.L. Yarin, Encapsulation of self-healing materials by coelectrospinning, emulsion electrospinning, solution blowing and intercalation, J. Mater. Chem. 22 (2012) 9138–9146, https://doi.org/10.1039/c2jm15696b.
[22] L. Wang, S.N. Li, J.J. Fu, Self-healing anti-corrosion coatings based on micron-nano containers with different structural morphologies, Prog. Org. Coat. 175 (2023) 107381, https://doi.org/10.1016/j.porgcoat.2022.107381.
[23] M.W. Lee, S. An, C. Lee, M. Liou, A.L. Yarin, S.S. Yoon, Hybrid self-healing matrix using core-shell nanofibers and capsuleless microdroplets, ACS Appl. Mater. Interfaces 6 (2014) 10461–10468, https://doi.org/10.1021/am5020293.
[24] A. Yabuki, A. Kawashima, I.W. Fathona, Self-healing polymer coatings with cellulose nanofibers served as pathways for the release of a corrosion inhibitor, Corros. Sci. 85 (2014) 141–146, https://doi.org/10.1016/j.corsci.2014.04.010.
[25] T.Q. Doan, L.S. Leslie, S.Y. Kim, R. Bhargava, S.R. White, N.R. Sottos, Characterization of core-shell microstructure and self-healing performance of electrospun fiber coatings, Polymer (Guildf) 107 (2016) 263–272, https://doi.org/10.1016/j.polymer.2016.10.062.
[26] D. Yan, Y. Wang, J. Liu, D. Song, T. Zhang, J. Liu, F. He, M. Zhang, J. Wang, Self-healing system adapted to different pH environments for active corrosion protection of magnesium alloy, J. Alloys Compd. 824 (2020) 153918, https://doi.org/10.1016/j.jallcom.2020.153918.
[27] X. Ji, W. Wang, X. Zhao, L. Wang, F. Ma, Y. Wang, J. Duan, B. Hou, Poly(dimethyl siloxane) anti-corrosion coating with wide pH-responsive and self-healing performance based on core−shell nanofiber containers, J. Mater. Sci. Technol. 101 (2022) 128–145, https://doi.org/10.1016/j. jmst.2021.06.014.
[28] G.E. Luckachan, V. Mittal, Self-healing anticorrosion coatings for gas pipelines and storage tanks, Corros. Sci. Technol. 15 (2016) 209–216, https://doi.org/10.14773/cst.2016.15.5.209.
[29] D. Snihirova, S.V. Lamaka, M.M. Cardoso, J.A.D. Condeço, H.E.C.S. Ferreira, M. De Fatima Montemor, pH-sensitive polymeric particles with increased inhibitor-loading capacity as smart additives for corrosion protective coatings for AA2024, Electrochim. Acta 145 (2014) 123–131, https://doi.org/10.1016/j.electacta.2014.09.009.
[30] Z. Tan, S. Wang, Z. Hu, W. Chen, Z. Qu, C. Xu, Q. Zhang, K. Wu, J. Shi, M. Lu, pH-responsive self-healing anticorrosion coating based on a lignin microsphere encapsulating inhibitor, Ind. Eng. Chem. Res. 59 (2020) 2657–2666, https://doi.org/10.1021/acs.iecr.9b05743.
[31] S.H. Cho, H.M. Andersson, S.R. White, N.R. Sottos, P.V. Braun, Polydimethylsiloxane-based self-healing materials, Adv. Mater. 18 (2006) 997–1000, https://doi.org/10.1002/adma.200501814.
[32] M. Huang, H. Zhang, J. Yang, Synthesis of organic silane microcapsules for self-healing corrosion resistant polymer coatings, Corros. Sci. 65 (2012) 561–566, https://doi.org/10.1016/j.corsci. 2012.08.020.
[33] S.J. Garcia, X. Wu, S. Van Der Zwaag, A combined electrochemical impedance spectroscopy and x-ray-computed tomography study of the effect of a silyl ester on delamination and underfilm pit formation in a coated AA7050 sample, Corrosion 70 (2014) 475–482, https://doi.org/10.5006/0966.
[34] Y. González-García, S.J. García, A.E. Hughes, J.M.C. Mol, A combined redox-competition and negative-feedback SECM study of self-healing anticorrosive coatings, Electrochem. Commun. 13 (2011) 1094–1097, https://doi.org/10.1016/j.elecom.2011.07.009.
[35] S.J. García, H.R. Fischer, P.A. White, J. Mardel, Y. González-García, J.M.C. Mol, A. E. Hughes, Self-healing anticorrosive organic coating based on an encapsulated water reactive silyl ester: synthesis and proof of concept, Prog. Org. Coat. 70 (2011) 142–149, https://doi.org/10.1016/j.porgcoat.2010.11.021.
[36] H. Kim, A.L. Yarin, M.W. Lee, Self-healing corrosion protection film for marine environment, Compos. Part B 182 (2020) 107598, https://doi.org/10.1016/j.compositesb.2019.107598.
[37] ISO 9227:2006(E), Corrosion Tests in Artificial Atmospheres — Salt Spray Tests, The International Organization for Standardization, Geneva, Switzerland, 2006.
[38] B.C. Smith, The C = O bond, part VI : esters and the rule of three, Spectroscopy 33 (2018) 20–23. https://www.spectroscopyonline.com/view/co-bond-part-vi-esters-and-rule-three.
[39] P.J. Launer, B. Arkles, Infrared analysis of organosilicon compounds: spectra-structure correlations, Silicon Compd. Silanes Silicones (2013) 175–178.
[40] E.A. Paukshtis, M.A. Yaranova, I.S. Batueva, B.S. Balzhinimaev, A FTIR study of silanol nests over mesoporous silicate materials, Microporous Mesoporous Mater. 288 (2019) 109582, https://doi.org/10.1016/j.micromeso.2019.109582.
[41] M.L. Zheludkevich, K.A. Yasakau, A.C. Bastos, O.V. Karavai, M.G.S. Ferreira, On the application of electrochemical impedance spectroscopy to study the self-healing properties of protective coatings, Electrochem. Commun. 9 (2007) 2622–2628, https://doi.org/10.1016/j.elecom.2007. 08.012.
[42] Y. Zuo, R. Pang, W. Li, J.P. Xiong, Y.M. Tang, The evaluation of coating performance by the variations of phase angles in middle and high frequency domains of EIS, Corros. Sci. 50 (2008) 3322–3328, https://doi.org/10.1016/j.corsci.2008.08.049.
[43] W. Tian, Z. Guo, S. Wang, H. Yu, S. Wang, H. Jin, L. Tian, Hydrogen and DA bond-based self-healing epoxy-modified polyurea composite coating with anti-cavitation, anticorrosion, antifouling, and strong adhesion properties, J. Mater. Sci. Technol. 187 (2024) 1–14, https://doi.org/10.1016/j.jmst.2023.11.031.
[44] H. Arabzadeh, M. Shahidi, M.M. Foroughi, Electrodeposited polypyrrole coatings on mild steel: modeling the EIS data with a new equivalent circuit and the influence of scan rate and cycle number on the corrosion protection, J. Electroanal. Chem. 807 (2017) 162–173, https://doi.org/10.1016/j.jelechem.2017.11.019.
[45] A. Trentin, A. Pakseresht, A. Duran, Y. Castro, D. Galusek, Electrochemical characterization of polymeric coatings for corrosion protection: a review of advances and perspectives, Polymers (Basel) 14 (2022) 1–28, https://doi.org/10.3390/polym14122306.
[46] W. Tian, H. Xu, Z. Guo, H. Yu, Y. Shang, L. Tian, Polyurethane coatings modified by OH-PDMS for anti-cavitation, antifouling and anticorrosion applications, Prog. Org. Coat. 179 (2023) 107515, https://doi.org/10.1016/j.porgcoat.2023.107515.
[47] G. Liu, Y. Zhang, M. Wu, R. Huang, Study of depassivation of carbon steel in simulated concrete pore solution using different equivalent circuits, Constr. Build. Mater. 157 (2017) 357–362, https://doi.org/10.1016/j.conbuildmat.2017.09.104.
[48] P.L. Bonora, F. Deflorian, L. Fedrizzi, Electrochemical impedance spectroscopy as a tool for investigating underpaint corrosion, Electrochim. Acta 41 (1996) 1073–1082.
[49] C. Lu, S. Mu, J. Du, K. Zhang, M. Guo, L. Chen, Investigation on the composition and corrosion resistance of cerium-based conversion treatment by alkaline methods on aluminum alloy 6063, RSC Adv. 10 (2020) 36654–36666, https://doi.org/10.1039/d0ra07201j.
[50] W. Tian, S. Wang, Z. Guo, H. Yu, L. Tian, Antifouling and anticorrosion function of repeatable self-healing polyurethane composite inspired by the self-healing principle of cartilage tissue, Chem. Eng. J. 462 (2023) 142346, https://doi.org/10.1016/j.cej.2023.142346.
[51] S.M. Gad, X. Zhou, S.B. Lyon, S. Emad, Effect of immersion time and pH variation on the inhibition of AA2198-T851 alloy by leaching of anticorrosion pigments from free-standing films of organic coatings, Results Mater. 16 (2022) 100335, https://doi.org/10.1016/j.rinma.2022.100335.
[52] S.V. Harb, A. Trentin, T.A.C. de Souza, M. Magnani, S.H. Pulcinelli, C.V. Santilli, P. Hammer, Effective corrosion protection by eco-friendly self-healing PMMA-cerium oxide coatings, Chem. Eng. J. 383 (2020) 123219, https://doi.org/10.1016/j.cej.2019.123219.
[53] X. Ji, W. Ji, S. Pourhashem, J. Duan, W. Wang, B. Hou, Novel superhydrophobic core-shell fibers/epoxy coatings with self-healing anti-corrosion properties in both acidic and alkaline environments, React. Funct. Polym. 187 (2023) 105574, https://doi.org/10.1016/j.reactfunctpolym.2023. 105574.
[54] C. Ma, J. Li, J. Wang, D. Bian, Y. Zhao, Self-healing corrosion-resistant coatings based on fluorinated alkyl silane microcapsules, Polym. Eng. Sci. 62 (2022) 4173–4184, https://doi.org/10.1002/pen.26176.
[55] W. Tian, S. Wang, C. Wang, H. Xu, Y. Zhao, H. Jin, L. Tian, An epoxy-modified polyurethane composite coating with repetitive self-healing function for anti-

cavitation, anticorrosion, and antifouling applications, Chem. Eng. J. 477 (2023) 146849, https://doi.org/10.1016/j.cej.2023.146849.
[56] S. Martinez, I. Šoić, V. Špada, Unified equivalent circuit of dielectric permittivity and porous coating formalisms for EIS probing of thick industrial grade coatings, Prog. Org. Coat. 153 (2021) 106155, https://doi.org/10.1016/j.porgcoat.2021.106155.
[57] I. Kunce, A. Królikowska, L. Komorowski, Accelerated corrosion tests in quality labels for powder coatings on galvanized steel—comparison of requirements and experimental evaluation, Materials (Basel) 14 (2021) 6547, https://doi.org/10.3390/ma14216547.
[58] G. Wu, J. An, D. Sun, X. Tang, Y. Xiang, J. Yang, Robust microcapsules with polyurea/silica hybrid shell for one-part self-healing anticorrosion coatings, J. Mater. Chem. A 2 (2014) 11614, https://doi.org/10.1039/c4ta01312c.
[59] Z. Sun, E. Zussman, A.L. Yarin, J.H. Wendorff, A. Greiner, Compound core-shell polymer nanofibers by co-electrospinning, Adv. Mater. 15 (2003) 1929–1932, https://doi.org/10.1002/adma.2003 05136.
[60] X. Wang, Q. Wang, F. Huang, Q. Wei, The morphology of Taylor cone influenced by different coaxial composite nozzle structures, Fibers Polym. 17 (2016) 624–629, https://doi.org/10.1007/s12221-016-5730-6.
[61] L. Cao, Q. Wang, W. Wang, Q. Li, S. Chen, Synthesis of smart nanofiber coatings with autonomous self-warning and self-healing functions, ACS Appl. Mater. Interfaces 14 (2022) 27168–27176, https://doi.org/10.1021/acsami.2c05048.